Propagation of Plasma Bullet in Impurity-Controlled Working Gas: from Standard to Ultrapure Atmospheric Pressure Plasma*)

Takumi HADA, Toshiki IKEDA, Mika YOSHIDA[1)], Katsuhisa KITANO[1)], Kei SHINADA[2)] and Mitsutoshi ARAMAKI

Nihon University, Narashino 275-8575, Japan
[1)]*Osaka University, Suita 565-0871, Japan*
[2)]*Shimadzu Corporation, Kyoto 619-0237, Japan*

(Received 10 January 2019 / Accepted 25 February 2019)

This study shows the variation of the characteristics of a plasma bullet generated in impurity controlled working gas. Tunable diode laser absorption spectroscopy of metastable He atoms generated in the plasma bullet was performed. The metastable He atoms are generated in the plasma bullet and are quenched by impurities. The velocity and the size of the plasma bullet are derived from the arriving time and the shape of the rising phase of the absorbance. In addition, the impurity concentration was derived from the decay time of the absorbance. The impurity concentration in the working gas is controlled in a range of more than two orders of magnitude, and the impurity concentration reaches ppb level. We have observed the impurity dependence of the velocity and size of the plasma bullet. The velocity of the plasma bullet reaches a constant value and the bullet size dramatically increase below 20 ppm of the impurities. These results show the change of the propagation mechanism of the plasma bullet in the high purity working gas. In order to distinguish the plasma generated in the high purity gas from the standard plasmas, we would call it ultrapure plasma.

Keywords: atmospheric pressure plasma, ultrapure plasma, plasma jet, plasma bullet, metastable helium atom, laser absorption spectroscopy

DOI: 10.1585/pfr.14.3406068

1. Introduction

Recently, atmospheric pressure plasma jet has been studied as a promising technology for the medical and biological applications. Although the plasma jet looks like a continuous discharge, it has been observed using an ICCD camera that plasma bullets are intermittently propagating. The several groups have reported the dependence of the velocity of the plasma bullet on the discharge conditions such as the peak voltage, frequency, waveform of the applied voltage and the permittivity of the material surrounding the plasma bullet [1–3]. In addition, the effect of the Penning ionization of impurities in the working gas has also been studied by several groups [4–11]. Most of these studies were performed by adding a few percent of the impurities molecules such as N_2 and O_2 to the standard purity working gas. In this study, the impurity concentration in the working gas is decreased from ppm to ppb order with gas purge and a purifier. The variation of the velocity and the size of the propagating plasma bullet is observed in the impurity controlled working gas. The bullet velocity in such a high purity working gas is firstly measured in this study. As far as we know, the dependence of the bullet size on the impurity concentration is also firstly reported. Since metastable atoms are generated in the plasma bullet and are quenched by the reaction with impurity molecules, the information of the plasma bullet and the concentration of the impurity is obtained from the spatiotemporal variation of the metastable atoms [12].

2. Experimental Setup

Figure 1 shows the experimental setup. A plasma jet is generated in a quartz tube (inner diameter 2 mm, outer diameter 4 mm, length 0.6 m) supported by the Bakelite holders. A copper foil (thickness 0.01 mm, width 15 mm) is wound outside the quartz tube as a discharge electrode and is powered with an AC high voltage power supply (Logy, LHV-10AC-24) at a frequency of 17 kHz with a peak voltage of 8 kV to generate plasma. The applied voltage and discharge current are measured using a high voltage probe (Tektronix, P6015) and a current transformer (Pearson electronics, MODEL110A), respectively. He gas is introduced from a high purity gas bomb (purity 99.99995%) into the quartz tube at 200 sccm via a mass flow controller (KOFLOC, MODEL8500) and a gas purifier (VICI, HP-2). Although the original purity of the gas bomb is high, the impurity concentration easily rises up to ppm level due to residual impurities. Therefore, the output of the gas purifier was directly connected to the dis-

author's e-mail: aramaki.mitsutoshi@nihon-u.ac.jp
*) This article is based on the presentation at the 27th International Toki Conference (ITC27) & the 13th Asia Pacific Plasma Theory Conference (APPTC2018).

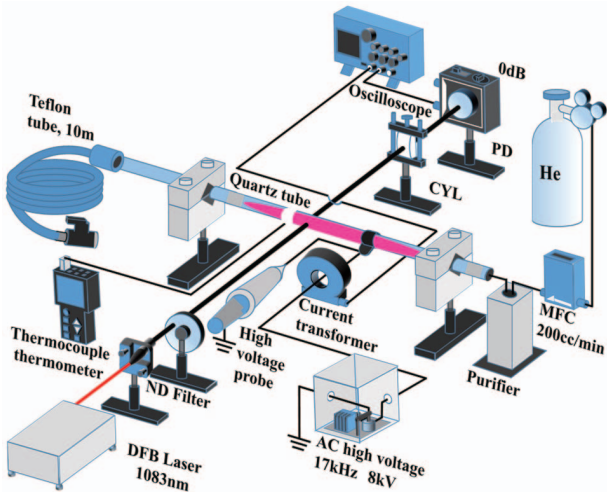

Fig. 1 (Color online) Experimental setup.

charge tube to supply high purity working gas. To prevent the back diffusion of impurities from the ambient air to the discharge area, a long Teflon tube (10 m) is connected to the end of the quartz tube. The temperature of the quartz tube is measured with a K type thermocouple attached to the quartz tube. By attaching the thermocouple, the plasma emission increased by approximately 2%. Therefore, the gas temperature might be overestimated a few percent higher. In this study, the influence of the overestimation was ignored. The thermocouple was removed when the spectroscopic measurements were carried out.

In this study, tunable diode laser absorption spectroscopy (TDLAS) is carried out to observe helium metastable atoms (2^3S_1) in the helium plasma jet using a distributed feedback (DFB) laser system. The DFB laser chip (TOPTICA, LD-1083-0070-DFB-1) is used for constructing the laser system. Although the tuning range of the DFB laser covers the three 2^3S-2^3P transitions (2^3S_1-2^3P_0, 2^3S_1-2^3P_1, 2^3S_1-2^3P_2) in the 1083-nm wavelength range, the wavelength of the DFB laser is fixed at the center of the absorption spectrum related to the 2^3S_1-2^3P_2 transition, since the absorption cross section of the transition is the largest among the three transitions [13]. The output power of the DFB laser was 50 mW at the experimental condition. The laser light is attenuated to 1 mW by the ND filter to prevent the saturation of the absorption and is perpendicularly incident to the discharge tube. The transmitted laser power is measured with an InGaAs photodiode detector (Thorlabs, PDA20CS). Since the transmitted light is diverged by the discharge tube, it is focused on the detector using a cylindrical lens. An interference filter is placed in front of the photo detector in order to remove unwanted plasma emissions and room lights and improve the signal-to-noise ratio. The output of the photo detector is recorded by a personal computer via the oscilloscope.

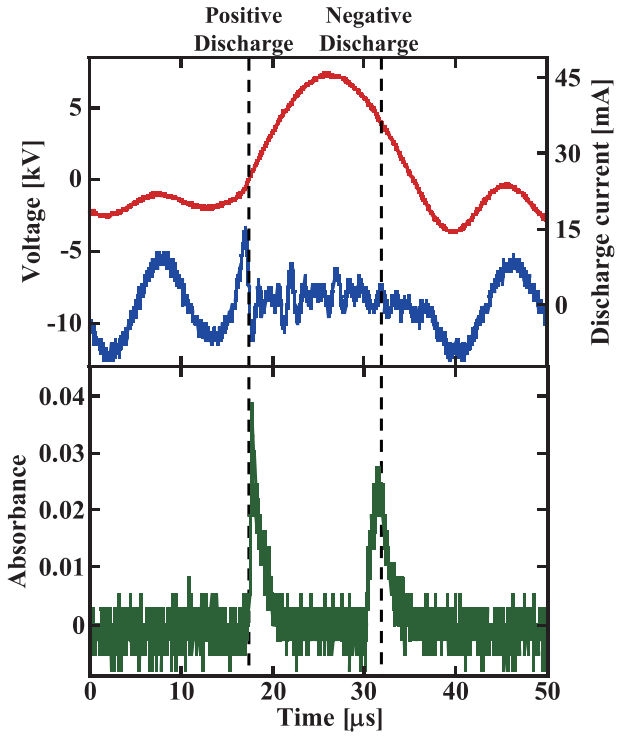

Fig. 2 (Color online) Waveforms of the applied voltage, discharge current and absorbance.

3. Results and Discussion

3.1 Analysis of absorbance waveform

Figure 2 shows the examples of the waveforms of the applied voltage, discharge current, and absorbance in one discharge cycle. The absorbance signal by He metastable atoms was observed beside the discharge electrode. Since the helium metastable density is low near the electrode, the absorbance is smaller than the data shown later. Although the absorbance signal clearly showed the occurrence of the positive and negative discharges at the rising and falling phase of the applied voltage, the discharge current of the negative discharge was small and difficult to see. In this article, the characteristics of the plasma jet generated by the positive discharge are studied. As reported by several research groups, the plasma jet is not continuous plasma but a discrete bullet-like plasma which is generated at the discharge front travelling at speeds of 10^4 m/s range [3, 14, 15]. Figure 3 shows an example of the temporal variation of the absorbance measured in a plasma jet generated with a standard purity He gas. Absorbance is calculated using the Lambert-Beer law

$$A = -\log_{10}\frac{I_T}{I_I},$$

where I_I and I_T are the intensity of the incident and the transmitted laser light, respectively. The horizontal axis shows the time after the positive discharge generation at the power electrode. The spectra were observed at the three positions where the distance from the power electrode was 2, 4, and 8 cm, respectively. Since the metastable He atoms

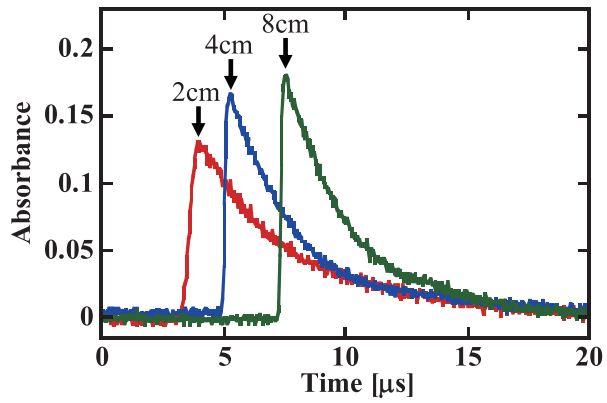

Fig. 3 (Color online) Spatiotemporal variation of pulsed absorption.

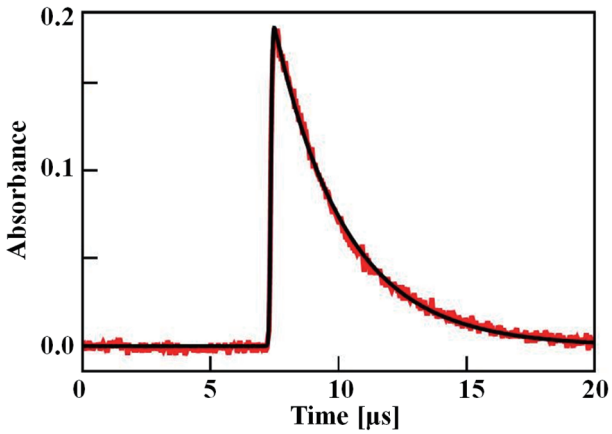

Fig. 4 (Color online) Waveform of the absorbance observed at 8 cm. τ_{He^*}, v_b, and L_b are derived as 2.8 μs, 11×10^3 m/s, 1.4 mm by fitting to Eq. (1), respectively.

are generated in the plasma bullet, the rapid increase of the absorbance means that the plasma bullet has reached the observation position. Therefore, the mean propagation velocity of the plasma bullet is derived by the distance from the power electrode and the rising time of the absorbance signal. In this case, the mean propagation velocity is roughly estimated as 10^4 m/s. In addition, the size of the plasma bullet is also derived from the shape of the rising phase. Peaking of the absorbance means passage of the plasma bullet, and from the decaying curve in the afterglow the information on the quenching process of the metastable He atoms is obtained. The absorbance signal was analyzed by fitting with Eq. (1).

$$\frac{dn_{He^*}}{dt} = n_{max} \exp\left(-\frac{\ln 2}{4}\frac{1}{L_b^2}(z - v_b t)^2\right) - \frac{n_{He^*}}{\tau_{He^*}}, \quad (1)$$

where n_{He^*} and τ_{He^*} are the density and decay time of metastable He atoms, respectively, n_{max} is the maximum value of the metastable He atom generation, and z is the distance from the power electrode. L_b is the full width at half maximum of the plasma bullet, and v_b is the propagation velocity of the plasma bullet. The density distribution of the plasma bullet is assumed to be a Gaussian function. The first term on the right side represents the metastable He atoms generation by the plasma bullet. The second term represents the quenching of metastable He atoms. Figure 4 shows a fitted curve with the waveform of the absorbance observed at 8 cm. τ_{He^*}, v_b, and L_b are derived as 2.8 μs, 11×10^3 m/s, 1.4 mm by fitting to Eq. (1), respectively. As far as we know, the quantitative evaluation of the bullet size has not been reported so far. However, the value of l_b is roughly the same order of magnitude as the size of the bullet images shown in Ref. [10].

After the plasma bullet passes through the observation point, the density of the metastable He atoms decreases by the transport and the quenching. In a pure He gas ambient, the metastable He atom is mainly quenched by the three-body collision with neutral He atoms, and is expressed by

$$He^* + 2He \rightarrow He_2^* + He, \quad (2)$$

and the decay time of He^* is given by

$$\tau_{He} = (K_3 \cdot n_{He}^2)^{-1}, \quad (3)$$

where n_{He} is the density of He atoms, the rate constant of the three-body collision K_3 is 2.5×10^{-34} cm^6 s^{-1} [16]. Since n_{He} greatly affects τ_{He}, the gas temperature dependence of n_{He} should be taken into account for the calculation of τ_{He}. Since the gas flow velocity is slow enough in this experiment, we assume that the He gas temperature is same with the quartz tube temperature. The temperature was 313 K at 8 cm from the power electrode and n_{He} is calculated as 2.34×10^{19} cm^{-3}. τ_{He} is calculated as 7.28 μs from the experimental conditions. Since the diffusion time of metastable He atoms to the wall is two orders of magnitude larger than τ_{He}, the quenching by the interaction with the inner wall of the discharge tube is negligible in this experiment. The Penning ionization of impurities is also an important process for quenching the metastable He atoms. Since the impurities contained in the gas bomb that was used in the experiment were mainly nitrogen and oxygen, the following Penning ionization processes of these species were taken into account in evaluating the decay time of the metastable He atoms:

$$He^* + N_2 \rightarrow He + N_2^+ + e, \quad (4)$$

and

$$He^* + O_2 \rightarrow He + O_2^+ + e. \quad (5)$$

The decay time of the metastable He atoms is modified by taking these process into account as follows,

$$\tau_{He,N2,O2} = (K_3 \cdot n_{He}^2 + K_{N2} \cdot n_{N2} + K_{O2} \cdot n_{O2})^{-1}, \quad (6)$$

where n_{N2} and n_{O2} are the density of the nitrogen and oxygen molecule. The rate constants of Penning ionization, K_{N2} and K_{O2} are 7.0×10^{-11} cm^3 s^{-1} and $2.5 \times$

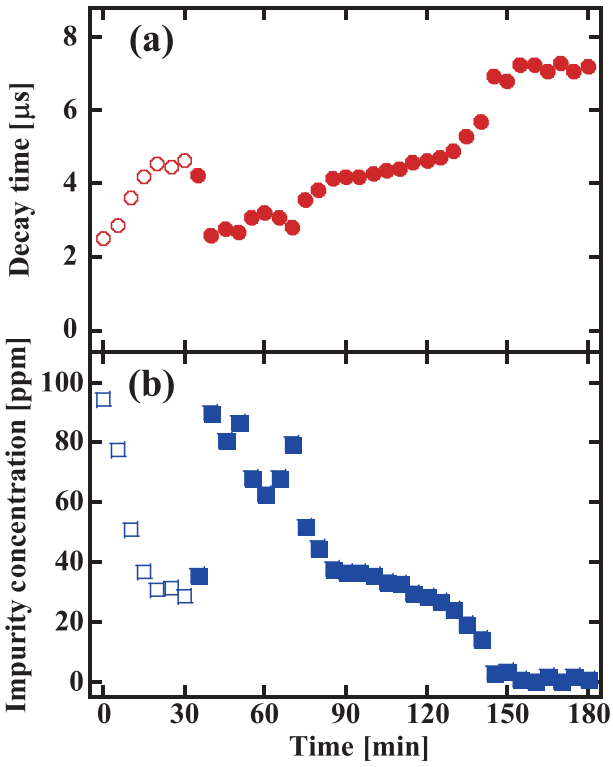

Fig. 5 (Color online) Temporal variation of (a) τ_{He^*} and (b) the impurity concentration. The closed symbols and open symbols show the data measured with and without purifier operation.

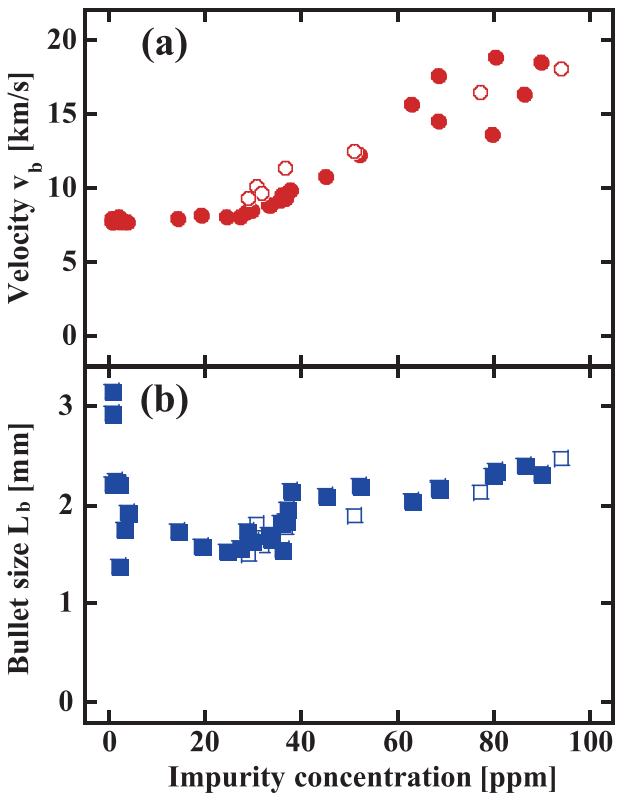

Fig. 6 (Color online) Impurity dependence of (a) v_b and (b) L_b. The closed symbols and open symbols show the data measured with and without purifier operation.

10^{-10} cm^3 s^{-1}, respectively [17, 18]. Since $\tau_{He,N2,O2}$ is obtained by the experiment and n_{He} is known, the impurity density is derived using Eq. (6). The mixing ratio of the nitrogen and the oxygen is assumed to be 8 : 2 same as in the air. In the case of the waveform shown in Fig. 4, the total impurity density ($n_{N2} + n_{O2}$) was derived as 91 ppm.

3.2 Impurity control

In the plasma jet experiment, the gas purity can be improved just by feeding fresh gas since the impurities are replaced by the high purity gas. In order to investigate the influence of the impurities in a wide range of concentrations, the purifier was used to further reduce the impurity concentration after the 30-minute He gas purge. After turning on the purifier, the impurity concentration in the He gas gradually decreased. The impurity concentration is derived using Eq. (6) and the experimentally obtained $\tau_{He,N2,O2}$. Figures 5 (a) and (b) shows the temporal variation of τ_{He^*} and the impurity concentration at 8 cm from the power electrode, respectively. The closed symbols and open symbols show the data measured with and without purifier operation. During the first 30 minutes, τ_{He} increased from 2.5 μs to 4.5 μs, and the impurity concentration decreased from 85 ppm to 25 ppm. After turning on the purifier, the impurities concentration increased once, but finally the impurity concentration decreased to 0.5 ppm. This experimental result shows that the impurity concentration can be varied in a range of more than two orders of magnitude by the gas purge and the purifier, and the impurity concentration can reach the ppb level.

3.3 Plasma bullet in impurity-controlled working gas

Figures 6 (a) and (b) shows the velocity v_b and size L_b of the plasma bullet propagating in the impurity-controlled working gas, respectively. The closed symbols and open symbols show the data measured with and without purifier operation. As shown in Fig. 6 (a), v_b monotonically increased with the impurity concentration above 20 ppm. This result is consistent with the numerical simulation by F. Liu *et al.* [9]. It is widely accepted that N_2^+ generated by the Penning ionization of N_2 in the working gas plays an important role in the propagation of the plasma bullet, and O_2 quenches the plasma bullet by capturing electrons [4–11]. The proportional relation between the impurity concentration and v_b also suggests that the Penning ionization processes shown in Eq. (4) might contribute to the variation of v_b. Several groups also observed the acceleration of the plasma bullets by the Penning ionization of N_2 in the standard purity gases. In this study, we firstly observed that v_b reaches the constant value (8×10^3 m/s) below 20 ppm. Although the dominant positive ion in the afterglow in the standard purity gas is N_2^+ [9], the composition of ions and the electron density might be changed in the ultrahigh pu-

rity working gas. Figure 6 (b) shows the dependency of L_b on the impurity concentration. L_b gradually increased with the impurity concentration above 20 ppm. The increase of the bullet size with the increase of the impurity concentration is also found in the photos in Ref. [10]. On the other hand, L_b dramatically increases when the impurity concentration decreased to 20 ppm or less. The variation of the bullet size with the impurity concentration has not been well studied below 20 ppm, and we believe that the reversal of the impurity concentration dependence of the bullet size was firstly observed in this study. In order to distinguish the plasma generated in the high purity gas from the standard plasmas, we would call it ultrapure plasma. Further study on the detail of the ultrapure plasma will be a future work.

In summary, we studied the characteristics of the plasma bullet generated in an impurity controlled working gas. TDLAS of the metastable He atoms generated in the plasma bullet was performed. From the decay time of the waveform of the absorbance, the impurity concentration was derived. In addition, the velocity and the size of the plasma bullet were obtained from the time and the shape of the rising phase of the absorbance. By using the gas purge and the purifier, the impurity concentration in the working gas was varied in a range of more than two orders of magnitude, and the impurity concentration reached the ppb level. We firstly observed that the velocity of the plasma bullet reached the constant value and the bullet size dramatically increased in the high purity working gas. Although further study on the detail of the ultrapure plasma will be a future work, these results show the change of the propagation mechanism of the plasma bullet in the high purity working gas.

Acknowledgement

This work was supported in part by the Grant-in-Aid for Scientific Research (B) 17H03000 from the Japan Society for the Promotion of Science (JSPS).

[1] N. Mericam-Bourdet, M. Laroussi, A. Begum and E. Karakas, J. Phys. D: Appl. Phys. **42**, 055207 (2009).
[2] J. Jansky and A. Bourdon, Appl. Phys. Lett. **99**, 161504 (2011).
[3] L. Ji, Y. Xia, Z. Bi, J. Niu and D. Liu, AIP Adv. **5**, 087181 (2015).
[4] K. Tachibana, Y. Kishimoto and O. Sakai, J. Appl. Phys. **97**, 123301 (2005).
[5] Y. Ito, K. Urabe, M. Kubo and K. Tachibana, Proc. 18th Int. Symp. On Plasma Chemistry (ISPC-18, Kyoto, Japan) 173 (2007).
[6] K. Urabe, Y. Ito, K. Tachibana and B.N. Ganguly, Appl. Phys. Express **1**, 066004 (2008).
[7] W.-C. Zhu, Q. Li, X.-M. Zhu and Y.-K. Pu, J. Phys. D: Appl. Phys. **42**, 202002 (2009).
[8] S. Wu, Q. Huang, Z. Wang and X. Lu, IEEE Trans. Plasma Sci. **39**, 2286 (2011).
[9] F. Liu, D. Zhang and D. Wang, Thin Solid Films **521**, 261 (2012).
[10] S. Wu, X. Lu and Y. Pan, Phys. Plasmas **21**, 073509 (2014).
[11] T. Shao, C. Zhang, R. Wang, Y. Zhou, Q. Xie and Z. Fang, IEEE Trans. Plasma Sci. **43**, 726 (2015).
[12] B. Niermann, A. Kanitz, M. Böke and J. Winter, J. Phys. D: Appl. Phys. **44**, 325201 (2011).
[13] A. Okamoto, K. Shinto, S. Kitajima and M. Sasao, Plasma Fusion Res. **2**, S1044 (2007).
[14] D. Maletic, N. Puac, G. Malovic, A. Dordevic and Z.L. Petrovic, J. Phys. D: Appl. Phys. **50**, 145202 (2017).
[15] R. Wang, Y. Gao, C. Zhang, P. Yan and T. Shao, IEEE Trans. Plasma Sci. **44**, 396 (2016).
[16] A.V. Phelps, Phys. Rev. **99**, 1307 (1955).
[17] T. Ueno and Y. Hatano, Chem. Phys. Let. **40**, 283 (1976).
[18] R.P. Cardoso, T. Belmonte, G. Henrion and N. Sadeghi, J. Phys. D Appl. Phys. **39**, 4178 (2006).